Quantum Mechanical Studies of the Photodissociation of Oxyheme Complexes

Ahmad Waleh* and Gilda H. Loew*

Contribution from the Molecular Theory Laboratory, The Rockefeller University, 701 Welch Road, Palo Alto, California 94304. *Received July 27, 1981*

Abstract: Semiempirical INDO-SCF-CI calculations were carried out on model oxyheme complexes in order to identify the photoactive states involved in the photodissociation of oxyhemoproteins. Excited-state energies and electron distributions were calculated as a function of iron-oxygen distance and were compared with similar calculations on carbonylheme complexes. The results were interpreted in terms of a two-channel photodissociation of oxygen above and below the Q band, respectively. The higher energy channel resembles the single channel available in the photodissociation of carbon monoxide in that in both complexes it proceeds through excited states of $d\pi \rightarrow d_{z^2}^*$ in nature. The lower channel involves excited charge-transfer states and does not have a parallel in the carbonylheme complexes. It is shown that competitive decays to lower excited states from the $d\pi \rightarrow d_{z^2}^*$ states involved in the higher energy channel and to the ground state from the excited states involved in the lower energy channel account for the low quantum yield of oxygen photodissociation. The proposed mechanism is consistent with and accounts for many of the features observed in picosecond photodissociation experiments.

Indentification of the photoactive excited states involved in the photodissociation of O_2 and CO derivatives of hemoglobin and myoglobin (HbO_2, MbO_2 and HbCO, MbCO) is of great interest for the study of the dynamics of ligand binding and energy relaxation mechanisms. Equally of interest is the determination of a mechanism of photodissociation derived from fundamental theoretical considerations of the ground and excited electronic states of both oxy- and carbon monoxyhemoproteins which is consistent with all the experimentally observed differences, as well as similarities, in their photodissociation properties.

Photodissociation studies with long duration pulses have long revealed the contrasting low quantum yield of O_2[1,2] as compared to that of CO.[2-6] More recent experiments in the time scales of microseconds[7-11] and nanoseconds[12-18] have provided valuable information about the dynamics of ligand binding and the nature of intermediates in the photodissociation of both ligands. Significant additional understanding of the ligand dissociation in hemoproteins is further provided by the picosecond studies[19-27] of the kinetics and the nature of primary events of the photoprocess. However, the dissociation mechanisms[19-26,28] advanced even on the basis of the interpretation of picosecond data have not been definitive, partly for lack of a comprehensive theoretical model, in accounting for all the experimental observations pertinent to both CO and O_2 photodissociations.

In the previous paper[29] (hereafter referred to as paper 1) we presented the results of a quantum mechanical study of the excited states of carbonylheme complexes as a function of Fe-CO distance and showed that the criterion of "decreasting excited-state energy with iron-ligand distance and no barrier to dissociation" leads to the unique identification of the states corresponding to $d\pi \rightarrow d_{z^2}^*$ transitions as the photoactive excited states. Moreover, it was shown that the calculated energies of these states are a function of the initial ligand geometry and for a bent Fe-C-O moiety representing hemoproteins, they are in the same energy range as the Q-band $\pi \rightarrow \pi^*$ transitions. A mechanism was thus proposed for the photodissociation of CO in terms of populating the singlet $d\pi \rightarrow d_{z^2}^*$ states, which would be photodissociating, either by direct excitation or by decay from higher energy singlet excited states. While not necessary for initiating dissociation, intersystem crossing to the triplet $d\pi \rightarrow d_{z^2}^*$ was suggested as one of the later events of the photoprocess. The mechanism deduced from this study is consistent with the observed high quantum yield of CO photodissociation[2-6] and its wavelength independence in the range of 280 to 620 nm.[4,28]

In this paper, we present the results of similar studies of the photodissociation of an oxyheme complex and show that the same criterion also leads to the identification of photodissociating channels in oxyhemoproteins and that the mechanisms of photodissociation of both O_2 and CO can be determined from consideration of the same principles. Calculations were thus made on the energies and electron distributions of the excited states of the oxyheme complex as a function of Fe-O_2 distance with the assumption of no change in spin or conformation. This assumption of a "frozen spin state", as in the case of the carbonylheme complex

(1) Q. H. Gibson and S. Ainsworth, *Nature (London)*, **180**, 1416 (1957).
(2) W. A. Saffran and Q. H. Gibson, *J. Biol. Chem.*, **252**, 7955 (1977).
(3) T. Bücher and E. Negelein, *Biochem. Z.*, **311**, 163 (1941).
(4) T. Bücher and J. Kaspers, *Biochim. Biophys. Acta* **1**, 21 (1947).
(5) R. W. Noble, M. Brunori, J. Wyman, and E. Antonini, *Biochemistry*, **6**, 1216 (1967).
(6) C. Bonaventura, J. Bonaventura, E. Antonini, M. Brunori, and J. Wyman, *Biochemistry*, **12**, 3424 (1973).
(7) R. H. Austin, K. W. Beeson, L. Eisenstein, H. Frauenfelder, and I. C. Gusalus, *Biochemistry*, **14**, 5355 (1975).
(8) N. Alberding, R. H. Austin, S. S. Chan, L. Eisenstien, H. Frauenfelder, I. C. Gunsalus, and T. M. Nordlund, *J. Chem. Phys.*, **65**, 4701 (1976).
(9) N. Alberding, S. S. Chan, L. Eisenstein, H. Frauenfelder, D. Good, I. C. Gunsalus, T. M. Nordlund, M. F. Perutz, A. H. Reynolds, and L. B. Sorensen, *Biochemistry*, **17**, 43 (1978).
(10) D. Beece, L. Eisenstein, H. Frauenfelder, D. Good, M. C. Marden, L. Reinisch, A. H. Reynolds, L. B. Sorensen, and K. T. Yue, *Biochemistry*, **18**, 3421 (1979).
(11) C. A. Sawicki and Q. H. Gibson, *J. Biol. Chem.*, **251**, 1533 (1976).
(12) B. Alpert, S. El Mohsni, L. Lindqvist, and F. Tfibel, *Chem. Phys. Lett.*, **64**, 11 (1979).
(13) D. A. Duddell, R. J. Morris, and J. T. Richards, *Biochim. Biophys. Acta*, **621**, 1 (1980).
(14) D. A. Duddell, R. J. *Morris*, N. J. Muttucumaru, J. T. Richards, *Photochem. Photobiol.*, **31**, 479 (1980).
(15) J. M. Friedman and K. B. Lyons, *Nature (London)*, **284**, 570 (1980).
(16) K. B. Lyons, J. M. Friedman, and P. A. Fleury, *Nature (London)* **275**, 565 (1978).
(17) R. F. Dallinger, J. R. Nestor, and T. G. Spiro, *J. Am. Chem. Soc.*, **100**, 6251 (1978).
(18) W. H. Woodruff and S. Farquharson, *Science (Washington, D.C.)*, **201**, 831 (1978).
(19) C. V. Shank, E. P. Ippen, and R. Bersohn, *Science (Washington, D.C.)*, **193**, 50 (1976).
(20) L. J. Noe, W. G. Eisert, and P. M. Rentzepis, *Proc. Natl. Acad. Sci. U.S.A.*, **75**, 573 (1978).
(21) W. G. Eisert, E. O. Degenkolb, L. J. *Noe*, and P. M. Rentzepis, *Biophys. J.*, **25**, 455 (1979).
(22) A. H. Reynolds, S. D. *rand*, and P. M. Rentzepis, *Proc. Natl. Acad. Sci. U.S.A.*, **78**, 2292 (1981).
(23) B. I. Greene, R. M. Hochstrasser, R. B. Weisman, and W. A. Eaton, *Proc. Natl. Acad. Sci. U.S.A.*, **75**, 5255 (1978).
(24) D. A. Chernoff, R. M. Hochstrasser, and A. W. Steele, Proc. *Natl. Acad. Sci. U.S.A.*, **77**, 5606 (1980).
(25) J. Terner, T. G. Spiro, M. Nagumo, M. F. Nicol, and M. A. El-Sayed, *J. Am. Chem. Soc.*, **102**, 3238 (1980).
(26) J. Terner, J. D. Stong, T. G. Spiro, M. Nagumo, M. Nicol, and M. A. El-Sayed, *Proc. Natl. Acad. Sci. U.S.A.*, **78**, 1313 (1981).
(27) M. Coppey, H. Tourbez, P. Valat, and B. alpert, *Nature (London)*, **284**, 568 (1980).
(28) B. M. Hoffman and Q. H. Gibson, *Proc. Natl. Acad. Sci. U.S.A.*, **75**, 21 (1978).
(29) A. Waleh and G. H. Loew, *J. Am. Chem. Soc.*, preceding paper in this issue.

0002-7863/82/1504-2352$01.25/0

Table I. Ground-State Orbital Description of Oxyheme Complex at Iron–Oxygen Distances of 1.75 and 2.17 Å[a]

orbital no.	Fe–O = 1.75 Å	Fe–O = 2.17 Å
92	99% a_{1u}*	100% a_{1u}*
91	(85% Imidσ, 12% Porphπ)*	(93% Imidσ, 1% d_{z^2})*
90	99% e_g*	100% e_g*
89	(88% e_g, 10% Imidσ)*	96% e_g*
88	100% b_{1u}*	(62% d_{xy}, 36% Porphσ)*
87	(55% d_{z^2}, 13% Porphσ, 13% Imidσ, 7% $O_2\sigma$, 4% d_{xy}, 2% $O_2\pi$)*	99% b_{1u}*
86	(58% d_{xy}, 34% Porphσ, 4% d_{z^2}, 1% $O_2\sigma$)*	(71% d_{z^2}, 13% Imidσ, 7% Porphσ, 3% $O_2\sigma$, 1% $O_2\pi$)*
85	(98% Imidπ, 1% d_{z^2})*	(99% Imidπ, 1% d_{z^2})*
84	100% b_{2u}*	100% b_{2u}*
83	99% Imidπ*	99% Imidπ*
82	(82% e_g, 12% d_{yz}, 5% $O_2\pi$)*	(98% e_g, 2% d_{yz})*
81	(99% e_g, 1% d_{xz})*	(98% e_g, 1% d_{xz})*
80	(43% $O_2\pi$, 36% d_{yz}, 18% e_g)*	(69% $O_2\pi$, 23% d_{yz}, 7% e_g)*
79	100% a_{1u}	96% a_{1u}, 4% $O_2\pi$, 1% d_{yz}
78	99% a_{2u}	99% a_{2u}
77	47% $O_2\pi$, 32% d_{yz}, 21% e_g	51% d_{yz}, 25% $O_2\pi$, 23% e_g
76	43% e_g, 34% d_{xz}, 12% $O_2\pi$, 7% $O_2\sigma$	50% e_g, 49% d_{xz}
75	36% Porphπ, 32% $O_2\pi$, 27% $O_2\sigma$, 1% d_{xz} 1% d_{z^2}, 1% $d_{x^2-y^2}$	94% $d_{x^2-y^2}$
74	82% b_{1u}, 18% Imidπ	68% b_{1u}, 32% Imidπ
73	87% a_{2u}, 5% $O_2\pi$, 3% $O_2\sigma$, 1% $d_{x^2-y^2}$	88% a_{2u}, 5% Imidπ, 3% $O_2\sigma$, 2% $O_2\pi$
72	69% Imidπ, 28% Porphπ, 1% $O_2\pi$, 1% $O_2\sigma$, 1% d_{xz}	53% Imidπ, 43% Porphπ, 1% d_{xz}
71	90% e_g, 3% $O_2\pi$, 3% d_{yz}	97% e_g, 1% d_{yz}
70	98% e_g	99% e_g
69	79% e_g, 7% d_{yz}, 6% $O_2\pi$, 3% $d_{x^2-y^2}$	75% e_g, 17% d_{yz}, 5% Imidπ, 2% $O_2\pi$
68	87% $d_{x^2-y^2}$, 6% Porphσ, 1% $O_2\pi$	40% e_g, 30% d_{xz}, 11% Imidπ, 11% $O_2\pi$, 7% $O_2\sigma$
67	48% d_{xz}, 27% e_g, 15% Imidπ, 7% $O_2\sigma$, 3% $O_2\pi$	39% $O_2\pi$, 35% $O_2\sigma$, 11% Porphπ, 9% d_{xz}

[a] Only the orbitals involved in the electronic transitions below and including Soret band are shown. Except for iron d, $O_2\pi$, and $O_2\sigma$ orbitals, all contributions below 5% are neglected. All symmetry designations refer to porphyrin π orbitals in D_{4h} symmetry.

(paper 1), makes these calculations relevant to the early bond-breaking events of photodissociation and is justifiable in the light of recent spectroscopic observations.[22,26]

Method

The calculations were carried out by using an INDO (intermediate neglect of differential overlap) program[30–33] which allows for the treatment of transition-metal complexes and the inclusion of extensive configuration interactions. The details of the program are described elsewhere.[34–36]

The geometry of the model oxyheme complexes used in this study with a bent end-on O_2 ligand is the same as the X-ray crystal

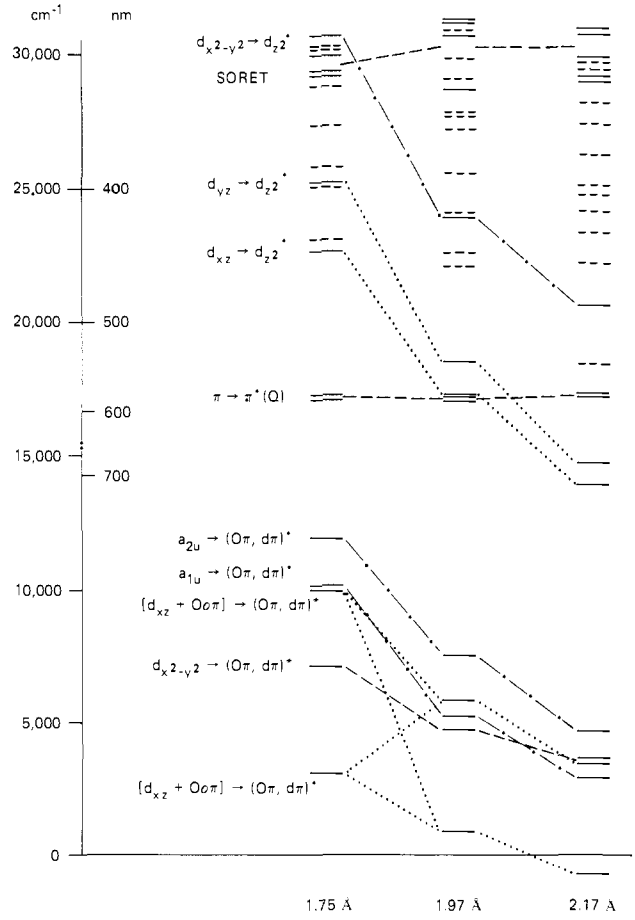

Figure 1. Simplified scaled diagramatic representation of the excited-state energies of the oxyheme complex at iron–oxygen distances of 1.75, 1.97, and 2.17 Å showing correlation between similar photodissociating states. The $\pi \rightarrow \pi^*$ transitions of the Soret and Q bands are also identified.

structure used in the previous calculations of oxyheme ground-state properties[37] and spectra,[34] except for variations in the Fe–O_2 distance along the axis perpendicular to the plane of porphyrin. In the coordinate system chosen, the pyrole nitrogen atoms bisect the *xy* axes, and therefore, the d_{xy} orbital becomes the "e_g" partner of d_{z^2}.

The ground- and excited-state electron distributions and energies were calculated at the three different Fe–O_2 distances of 1.75, 1.97, and 2.17 Å. SCF–MO–LCAO level calculations were performed on each of the geometries described above by using an INDO/1 approximation with the two-center repulsion integrals evaluated using an empirical Weiss–Mataga–Nishimoto formula.[38,39] Excited-state energies were calculated by performing single excitation configuration interaction computations on the SCF level eigenvectors. A total of 207 single excitation configurations were used in each case corresponding to excitations from 15 highest occupied orbitals into 13 lowest virtual orbitals and a small set of 12 configurations involving a few remaining low-lying orbitals with minor iron d characters.

Results

Table I shows the ground-state atomic orbital composition of the principal molecular orbitals used in the configuration interaction calculations of the oxyheme complex at iron–oxygen distances of 1.75 and, for comparison, 2.17 Å. The major components of the calculated excited states, below and including the Soret band, are given in Table II at iron–ligand distances of 1.75, 1.97,

(30) J. Ridley and M. Zerner, *Theor. Chim. Acta*, **32**, 111 (1973).
(31) J. E. Ridley and M. C. Zerner, *Theor. Chim. Acta*. **42**, 223 (1976).
(32) A.D. Bacon, PhD. dissertation, Department of Chemistry, University of Guelph, Canada, 1976.
(33) A. D. Bacon and M. C. Zerner, *Theor. Chim. Acta*, **53**, 21 (1979).
(34) G. H. Loew, Z. S. Herman, and M. C. Zerner, *Int. J. Quantum Chem.*, **18**, 481 (1980).
(35) Z. S. Herman, G. H. Loew, and M. M. Rohmer, *Int. J. Quantum Chem., Quantum Biol. Symp.*, **7**, 137 (1980).
(36) M. C. Zerner, G. H. Loew, R. F. Kirchner, and U. T. Mueller-Westerhoff, *J. Am. Chem. Soc.*, **102**, 589 (1980).
(37) Z. S. Herman and G. H. Loew, *J. Am. Chem. Soc.*, **102**, 1815 (1980).
(38) K. Weiss, unpublished.
(39) N. Mataga and K. Nishimoto, *Z. Phys. Chem. (Wiesbaden)*, **13**, 140 (1957).

Table II. Calculated Excited States of Oxyheme Complex as a Function of Iron-Oxygen Distance

Fe-O = 1.77 Å		Fe-O = 1.97 Å		Fe-O = 2.17 Å	
frequency,[a] cm^{-1}	major components[b,c]	frequency, cm^{-1}	major components[b,c]	frequency, cm^{-1}	major components[b,c]
3 111	$(d_{xz};O\sigma\pi) \rightarrow (O\pi,d_{yz})$ (97%)	979	$O\sigma\pi; d_{xz}; a_{2u} \rightarrow (O\pi,d_{yz})^*$ (72%; 19%; 6%)	695	$O\sigma\pi; a_{2u}; d_{xz} \rightarrow (O\pi,d_{yz})^*$ (79%; 11%; 6%)
7 119	$d_{x^2-y^2}; O\sigma\pi \rightarrow (O\pi,d_{yz})^*$ (88%; 6%)	4 722	$d_{x^2-y^2}; d_{xz} \rightarrow (O\pi,d_{yz})^*$ (87%; 9%)	2 954	$a_{1u} \rightarrow (O\pi,d_{yz})^*$ (96%)
9 955 (0.0004; xy)	$(d_{xz}; O\sigma\pi); a_{2u}; d_{x^2-y^2} \rightarrow (O\pi,d_{yz})^*$ (74%; 14%; 5%)	5 238	$a_{1u} \rightarrow (O\pi,d_{yz})^*$ (99%)	3 446	$d_{x^2-y^2}; d_{xz}; a_{2u} \rightarrow (O\pi,d_{yz})^*$ (48%; 44%; 5%)
10 172 (0.008; x)	$a_{1u} \rightarrow (O\pi,d_{yz})^*$ (96%)	5 884	$d_{xz}; a_{2u}; d_{x^2-y^2} \rightarrow (O\pi,d_{yz})^*$ (65%; 17%; 7%)	3 642	$d_{x^2-y^2}; d_{xz}; a_{2u} \rightarrow (O\pi,d_{yz})^*$ (46%; 30%; 22%)
11 899 (0.002; y)	$a_{2u}; O\sigma\pi \rightarrow (O\pi,d_{yz})^*$ (79%; 19%)	7 562	$a_{2u}; O\sigma\pi, d_{xz} \rightarrow (O\pi,d_{yz})^*$ (74%; 14%; 9%)	4 647	$a_{2u}, O\sigma\pi, d_{xz} \rightarrow (O\pi,d_{yz})^*$ (60%; 22%; 14%)
				13 842	$d_{xz} \rightarrow d_{z^2}^*$ (90%)
				14 613	$d_{yz} \rightarrow d_{z^2}^*$ (89%)
17 115 (0.041; xy)	$a_{1u}; a_{2u} \rightarrow e_g^*$ (58%; 38%)	17 061	$a_{1u}; a_{2u} \rightarrow e_g^*$ (60%; 38%)	17 150	$a_{1u}; a_{2u} \rightarrow e_g^*$ (61%; 35%)
17 177 (0.051 xy)	$a_{1u}; a_{2u} \rightarrow e_g^*$ (59%; 37%)	17 100	$a_{1u}; a_{2u} \rightarrow e_g^*$ (59%; 37%)	17 195	$a_{1u}; a_{2u} \rightarrow e_g^*$ (61%; 36%)
		17 225	$d_{xz} \rightarrow d_{z^2}^*$ (92%)		
		18 431	$d_{yz} \rightarrow d_{z^2}^*$ (91%)		
				18 327	$d_{yz} \rightarrow (O\pi,d_{yz})^*$ (67%); $d_{x^2-y^2} \rightarrow d_{z^2}^*$ (28%)
22 636 (0.017; z)	$d_{xz} \rightarrow d_{z^2}^*$ (79%); $d_{yz} \rightarrow (O\pi,d_{yz})^*$ (11%)	22 078	$d_{yz} \rightarrow (O\pi,d_{yz})^*$ (82%); $d_{x^2-y^2} \rightarrow d_{z^2}^*$ (10%)	20 531	$d_{x^2-y^2} \rightarrow d_{z^2}^*$ (66%); $d_{yz} \rightarrow (O\pi,d_{yz})^*$ (30%)
23 087	$d_{x^2-y^2} \rightarrow d_{xy}^*$ (98%)	22 525	$d_{x^2-y^2} \rightarrow d_{xy}^*$ (96%)	22 158	$d_{x^2-y^2} \rightarrow d_{xy}^*$ (96%)
25 090 (0.191; z)	$d_{yz} \rightarrow (O\pi,d_{yz})^*$ (76%); $d_{xz} \rightarrow d_{z^2}^*$ (16%)	23 866	$d_{x^2-y^2} \rightarrow d_{z^2}^*$ (84%); $d_{yz} \rightarrow (O\pi,d_{yz})^*$ (10%)		
25 209 (0.003; z)	$d_{yz} \rightarrow d_{z^2}^*$ (55%); $d_{xz} \rightarrow d_{xy}^*$ (39%)				
25 807 (0.001; yz)	$d_{yz} \rightarrow e_g^*$ (96%)	24 040	$d_{yz} \rightarrow e_g^*$ (97%)	23 284	$d_{yz} \rightarrow e_g^*$ (94%)
27 383 (0.053; xz)	$d_{yz}; d_{xz} \rightarrow e_g^*$ (83%; 9%)	25 513	$d_{yz}; d_{xz} \rightarrow e_g^*$ (90%; 3%)	24 085	$b_{1u} \rightarrow (O\pi,d_{yz})^*$ (79%); $d_{yz} \rightarrow e_g^*$ (10%)
28 791 (0.065; xy)	$a_{1u} \rightarrow \text{Imid}\pi^*$ 95%	27 150	$b_{1u} \rightarrow (O\pi,d_{yz})^*$ (73%); $a_{1u}; a_{2u} \rightarrow e_g^*$ (7%; 14%)	24 678	$d_{yz} \rightarrow e_g^*$ (85%); $b_{1u} \rightarrow (O\pi,d_{yz})^*$ (10%)
		27 261	$d_{yz} \rightarrow d_{xy}^*$ (87%)	25 020	$d_{xz} \rightarrow (O\pi,d_{yz})^*$ (56%); . . .
29 166 (1.415; xy)	$a_{1u}; a_{2u} \rightarrow e_g^*$ (37%; 23%); . . .	27 783	$a_{1u}; a_{2u} \rightarrow e_g^*$ (2%; 5%); . . .	26 188	$a_{1u}; a_{2u} \rightarrow e_g^*$ (2%; 8%); . . .
29 310 (1.390; xy)	$a_{1u}; a_{2u} \rightarrow e_g^*$ (38%; 23%); $d_{yz} \rightarrow d_{z^2}^*$ (10%); . . .	28 613	$a_{1u}; a_{2u} \rightarrow e_g^*$ (11%; 22%); . . .	27 357	$d_{yz} \rightarrow d_{xy}^*$ (90%)
29 930 (0.585; xy)	$a_{1u}; a_{2u} \rightarrow e_g^*$ (15%; 9%); $d_{yz} \rightarrow d_{z^2}^*$ (16%); . . .	28 997	$a_{1u} \rightarrow \text{Imid}\pi^*$ (97%)	28 121	$d_{yz} \rightarrow (O\pi,d_{yz})^*$ (38%); $a_{1u}; a_{2u} \rightarrow e_g^*$ (4%); . . .
30 148 (0.013; xyz)	$d_{xz} \rightarrow (O\pi,d_{yz})^*$ (60%); . . .	29 759	$d_{xz} \rightarrow d_{xy}^*$ (88%); $d_{yz} \rightarrow d_{z^2}^*$ (6%)	28 889	$d_{xz} \rightarrow e_g^*$ (55%); $e_g \rightarrow e_g^*$ (24%)
30 258 (0.108; xyz)	$d_{yz} \rightarrow d_{xy}^*; d_{z^2}^*$ (44: 19%); . . .	30 610	$a_{1u}; a_{2u} \rightarrow e_g^*$ (21%; 29%); . . .	29 101	$a_{1u}; a_{2u} \rightarrow e_g^*$ (9%; 15%); . . .
30 686 (0.112; xy)	$d_{x^2-y^2} \rightarrow d_{z^2}^*$ (79%); . . .	30 798	$d_{xz} \rightarrow e_g^*$ (39%); $a_{1u} \rightarrow b_{2u}^*$ (27%); . . .	29 392	$a_{1u}; a_{2u} \rightarrow e_g^*$ (9%; 14%); . . .
		31 106	$a_{1u}; a_{2u} \rightarrow e_g^*$ (9%; 12%); . . .	29 653	$d_{xz} \rightarrow d_{xy}^*$ (88%)
		31 178	$a_{1u}; a_{2u} \rightarrow e_g^*$ (15%; 17%); . . .	29 773	$a_{1u} \rightarrow \text{Imid}\pi^*$ (93%)
		31 710	$a_{1u}; a_{2u} \rightarrow e_g^*$ (3%; 4%); . . .	30 638	$a_{1u}; a_{2u} \rightarrow e_g^*$ (13%; 20%); . . .
				30 895	$a_{1u}; a_{2u} \rightarrow e_g^*$ (13%; 33%); . . .
				31 250	$a_{1u}; a_{2u} \rightarrow e_g^*$ (8%; 13%); . . .

[a] Nonzero oscillator strengths and polarizations are given in parentheses. [b] See text for orbital notations. [c] For the excited states corresponding to the Soret band, only $a_{1u}, a_{2u} \rightarrow e_g^*$ components are given.

and 2.17 Å. A simplified scaled diagramatic representation of the excited-state energies is also shown in Figure 1. It should be noted that the atomic orbital notations used to specify the transitions in Table II represent only the main character, and not the entire composition, of the molecular orbitals involved. In addition to the main orbital character, the remaining orbital character can be obtained by examining Table I for the atomic orbital compositions of the molecular orbitals involved in the transitions. For example, as can be seen from Table I, the iron d_{xz} and d_{yz} orbitals are generally mixed with porphyrin e_g and oxygen π orbitals, and the transitions labeled by $d_{xz} \rightarrow$ or $d_{yz} \rightarrow$ thus have e_g and $O\pi$ characters as well. Also the transitions labeled by $O\sigma\pi$, chosen for brevity in Table II, are those involving molecular orbitals which contain both $O\pi$ and $O\sigma$ contributions (see Table I), and the degree of mixing of these orbitals is roughly proportional to their percentage of $O\pi$ and $O\sigma$ characters.

It is readily evident from both Table II and Figure 1 that, according to our criterion of "decreasing energy with increasing iron–ligand distance and no barrier to dissociation", two groups of dissociating states can be recognized. The first group comprises $d\pi \rightarrow d_{z^2}^*$ and $d_{x^2-y^2} \rightarrow d_{z^2}^*$ transtions which, at bonding iron–oxygen distance (1.75 Å), lies above the Q band. The second group comprises some or all of the charge-transfer states that lie below the Q band. It is difficult to single out a given state of this group as the primary dissociating state since the semiempirical calculations of energy profile become complicated at longer iron–oxygen distances as oxygen becomes more atomic in character. The crossing of the first excited state below the reference ground state at Fe–O = 2.17 Å may be an artifact, since the closed-shell reference ground state, at the present level of these calculations, does not include doubly excited configurations which are known from our previous work to be important in oxyheme.[37] In any case, we note that of all the low-lying states, the charge-transfer states corresponding to a $a_{1u} \rightarrow (O\pi, d_{yz})^*$ and $a_{2u} \rightarrow (O\pi,d_{yz})^*$ transitions display the steepest energy profile with increasing iron–ligand distance.

Discussion

The major conclusion of the present study, as can be seen from the results presented in Table II and Figure 1, is the presence of two dissociating channels in oxyheme, one lying above and one lying below the energy of the $\pi \rightarrow \pi^*$ transitions of the Q band. This is in contrast to the pattern calculated for the carbonylheme complex (paper 1) where only one such dissociating channel was recognized.

The channel of higher energy than the Q band consists of the states corresponding to $d\pi \rightarrow d_{z^2}$ and $d_{x^2-y^2} \rightarrow d_{z^2}^*$ transitions. The same states also displayed a dissociating profile in carbonylheme complex except that, for bent Fe–C–O geometry representing carbon monoxyhemoproteins, the energies of the states corresponding to $d\pi \rightarrow d_{z^2}^*$ transitions were calculated in the same range as the Q band transitions at iron–carbon bonding distance of 1.77 Å (see Figure 2 of paper 1). The calculated energies of $d\pi \rightarrow d_{z^2}^*$ transitions in oxyheme are clearly much higher than the Q-band $\pi \rightarrow \pi^*$ transitions. The difference in the relative positions of $d\pi \rightarrow d_{z^2}^*$ transitions with respect to the Q band in carbonylheme and oxyheme complexes is not due to the slightly shorter Fe–O bond length of 1.75 Å in oxyheme as compared to Fe–C bond length of 1.77 Å in carbonylheme. Figure 1 shows that Fe–O distance can be stretched by a full 0.22 Å before the energies of the $d\pi \rightarrow d_{z^2}^*$ transitions are lowered to the same range as that of the Q band. Furthermore, the calculated excited-state energies of oxyheme are in general agreement with the assignments of the observed bands in HbO_2.[40] We, therefore, believe that the calculated differences in energies of the $d\pi \rightarrow d_{z^2}$ transitions in oxyheme and carbonylheme complexes are genuine in nature and, as will be shown below, partially account for the difference in their photodissociation properties. Following the arguments presented in paper 1, the states corresponding to $d\pi \rightarrow d_{z^2}^*$ transitions are identified as the main dissociating states above the Q band of oxyhemoproteins.

An interesting aspect of the present calculations is the dissociating nature of the charge-transfer states of oxyheme which lie below the Q band. These excited states are absent from carbonylheme spectra. On the basis of the steepness of the energy profile only (see Figure 1), the two states corresponding to $a_{1u} \rightarrow (O\pi,d\pi)^*$ and $a_{2u} \rightarrow (O\pi,d\pi)^*$ transitions are favored as the photoactive states. However, because of the low energies involved, the remaining charge-transfer states can also be dissociating and some or all may provide a nonradiative decay channel through coupling to the ground state.

The results of the present study, relevant to oxyhemoproteins, and those for the bent carbonylheme complex (paper 1), relevant to carbon monoxyhemoproteins, enable us to formulate consistent mechanisms for O_2 and CO photodissociations that can account for the relevant observed behavior of both ligands. Because of our assumption of a "frozen spin state" and frozen geometries in these calculations, our results apply only to the primary events of the photodissociation process occurring in the time scale of picoseconds. Thus our results are used to interpret only picosecond data.

The major results of our studies of oxy- and carbon monoxyhemoproteins can be summarized as follows. (1) The states corresponding to $d\pi \rightarrow d_{z^2}^*$ transitions form a dissociating channel in both complexes. (2) While this channel lies above the Q band for the O_2 ligand, it lies below the Q band for the CO ligand. (3) Charge-transfer states in the oxy complex form a second dissociating channel below the Q band which is absent in the carbon monoxy case. (4) In neither case are the $\pi \rightarrow \pi^*$ transitions dissociating in nature. We further assume that there is a nonradiative decay channel from the charge-transfer states to the ground state of oxyheme. A simplified schematic representation of the channels involved in the photodissociation of oxy- and monoxyhemoproteins is shown in Figure 2.

The mechanism of CO photodissociation is quite straightforward, since there is only one dissociation channel, involving singlet

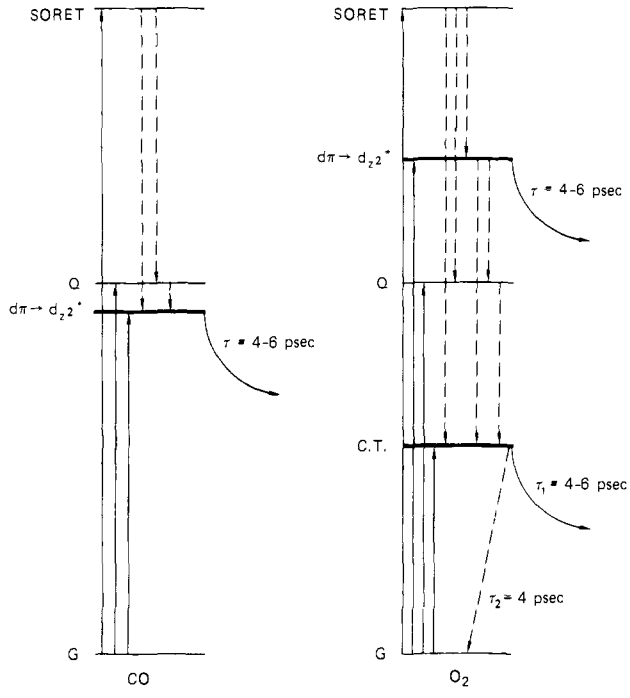

Figure 2. Simplified schematic representation showing two-channel photodissociation of oxyhemoproteins vs. single-channel photodissociation of carbon monoxyhemoproteins. Vertical solid and dashed lines represent excitations and nonradiative decays, respectively. The dissociation lifetimes are taken from ref 22, and the decay lifetime, τ_2, from charge-transfer states (CT) to the ground state (G) is estimated in this work.

$d\pi \rightarrow d_{z^2}^*$ states, which lies below both the Soret and Q bands. This mechanism is consistent with the observations of high quantum yield[2-6] for CO and its wavelength independence.[4,28] Dissociation here refers to the first event of the photoprocess; that is, other events such as spin conversion or intermediate formation are considered to occur as subsequent events. It was shown in paper 1 that the possibility of intersystem crossing to a triplet $d\pi \rightarrow d_{z^2}^*$ as the next immediate event of photodissociation is consistent with our calculations.

O_2 photodissociation, on the other hand, appears to occur through two independent channels. The upper channel corresponds to singlet $d\pi \rightarrow d_{z^2}^*$, similar to the channel available in the CO complex, except that, by virtue of its energy being higher than that of the Q band, it is only accessible by either direct excitation from the ground state or decay from the Soret band. The lower channel, however, which may consist of a manifold of charge-transfer states, is accessible either by direct excitation or decay from all higher energy singlet excited states. The presence of a single dissociation channel in carbonylheme and two channels, each of different nature, in oxyheme is consistent with the observations of Green et al.[23] and Chernoff et al.[24] that photolysis of HbCO yields similar transient spectra when induced at 353[23] and 530 nm[24] while that of HbO_2 results in a different transient spectra for each of the two excitation wavelengths. More specifically, the observation that when HbO_2 is excited at 353 nm its initial (10 ps) kinetics and spectrum are similar to that of HbCO[23] is also in agreement with our result that the upper channel of oxyheme involves the same $d\pi \rightarrow d_{z^2}^*$ excited states as the carbonylheme complex. Moreover, the difference in kinetics and transient spectra of the 530-nm induced photoproducts of HbCO and HbO_2[24] is indicative of the different nature of the dissociation channels below the Q band of the two liganded hemoproteins.

Further support of the proposed two-channel mechanism of photodissociation in oxyheme comes from the observed dependence of the quantum yield on excitation frequency. In the interesting work of Reynolds et al.,[22] it was observed that the quantum yield of MbO_2, in the time range of 4–12 ps after photodissociation, is approximately 0.3 and 0.1 when excited at 355 and 530 nm, respectively. They have also estimated a lifetime of 4–6 ps,

(40) W. A. Eaton, L. K. Hanson, P. J. Stephens, J. C. Sutherland, and J. B. R. Dunn, *J. Am. Chem. Soc.*, **100**, 4991 (1978).

probably an upper limit, for the kinetics of disappearance of MbO_2 and MbCO, independent of the excitation energy. As can be seen from Figure 2, excitation at 355 nm results in dissociation from both channels while 530-nm excitation can utilize only one channel and, therefore, results in a lower quantum yield.

If the charge-transfer manifold in oxyheme were not coupled to the ground state, the dissociative nature of these states would have resulted in quantum yield of unity. Indeed the existence of a nonradiative decay channel, as shown in Figure 2, together with the dissociative nature of the charge-transfer states, is responsible for the simultaneous ready photolability and low quantum yield of oxyhemoproteins. Assuming only a single dissociating charge-transfer state below the Q band and also assuming simple exponential kinetics for both dissociation and decay out of this state, we calculate[41] a quantum yield of 0.25 if we assume dissociation and decay lifetime values of 6 and 4 ps (see Figure 2), respectively. This value is not far from the observed value of about 0.1. While neither value is accurately determined, the difference may indicate that the lower dissociation channel in oxyheme is more complicated than a single dissociating state and that the decay mechanism is not a simple exponential. The same simple model also gives a lifetime of about 2.4 ps for the depletion of the charge-transfer state. This provides an explanation for the observation of Shank et al.[19] that their excitation of HbO_2 at 615 nm resulted in an induced signal that decayed with a time constant of 2.5 ps. If we consider the 2.5 ps as a lower limit to the depletion of the dissociating state, it follows that neither the dissociation nor the decay lifetime can be less than 2.5 ps, and therefore, the 0.5-ps rise time of their induced signal cannot be a lower limit to photodissociation lifetime in HbO_2. We thus tend to agree with the suggestion[20] that HbO_2 was excited into a dissociating state by the 615-nm subpicosecond pulse used, and the new species was monitored until depletion.

Finally we should point out that our results are at variance with the conclusion reached by Hoffman and Gibson[28] that the low quantum yield of HbO_2 is due to radiationless decay to charge-transfer states which they consider both short lived and stable. We rather assert that these states themselves are photodissociating and that the low quantum yield of HbO_2 results from the competing dissociation and decay kinetics which holds true for both upper and lower channels.

(41) Assuming a simple two-state model below the Q band, and assuming simultaneous exponential dissociation to an intermediate state I with a lifetime of $\tau_1 = 6$ ps and a decay to the ground state with a lifetime of $\tau_2 = 4$ ps, similar to that shown in Figure 2 of the text, we can write

$$n(t) = n_0 \exp(-t/\tau_{dep});\ \tau_{dep} = \tau_1\tau_2/(\tau_1 + \tau_2)$$

where n_0 is the population of the initially excited states near the saturation level and $n(t)$ is the population at time t with depletion time constant of $\tau_{dep} = 2.4$ ps. If $n_1(t)$ is the population of the intermediate species resulting from dissociation, it is straightforward to show that

$$n_1(t) = (n_0\tau_{dep}/\tau_1)[1 - \exp(-t/\tau_{dep})]$$

The quantum yield of dissociation in the time scale of depletion lifetime of the dissociating state is given by

$$\phi = n_1(\tau_{dep})/n_0 = \tau_1(1 - e^{-1})/(\tau_1 + \tau_2) = 0.25$$

for $\tau_1 = 6$ and $\tau_2 = 4$ ps.

Conclusion

Single configuration interaction calculations of the excited states of oxyheme complex as a function of iron–ligand distance have been made and the results used to establish that the photodissociation of oxyhemoproteins occurs through two independent channels, one above and one below the Q band in energy. The upper channel involves $d\pi \rightarrow d_{z^2}^*$ photoexcited states and thus resembles the only dissociation channel available to carbon monoxyhemoproteins, most likely with similar kinetics. The lower channel involves charge-transfer excited states and is specific for oxyhemoproteins. Mechanisms have been proposed for the photodissociation of O_2 and CO which are consistent with the picosecond experimental data. It is found that the low quantum yield of oxyhemoprotein at low excitation energies is due to competitive decay from dissociative charge-transfer states and at high excitation energies is due to nonradiative decay to singlet states below the dissociative $d\pi \rightarrow d_{z^2}^*$ channel.

Acknowledgment. We gratefully acknowledge financial support for this work from NSF Grant PCM-7921591. We also thank Dr. Dale Spangler for many helpful discussions during the course of this work and Brenda Wells for help in preparation of the manuscript.

Mechanism of Cobalt(III)-Promoted Hydrolysis of Triphosphate Ion

Paul R. Norman and Richard D. Cornelius*

Contribution from the Department of Chemistry, Wichita State University, Wichita, Kansas 67208. *Received July 15, 1981*

Abstract: The mechanism of hydrolysis of phosphates has been studied by using the well-characterized complex β,γ-$[Co(NH_3)_4H_2P_3O_{10}]$, in which the triphosphate ion is coordinated as a bidentate ligand. The rate of hydrolysis of the triphosphate ion to pyrophosphate ion in this complex has been studied in the presence of the cobalt(III) complex of the macrocyclic tetraamine ligand, cyclen. In the presence of this macrocyclic complex, the rate of hydrolysis was increased by 5×10^5 over the rate for the free triphosphate ion. The dependence of the rate upon pH showed that a deprotonation step with a pK of 7.9 was critical for the accelerated hydrolysis to occur. The results are consistent with a mechanism involving coordination of the free end of the phosphate chain in the $Co(NH_3)_4H_2P_3O_{10}$ by the cyclen complex to form a dinuclear species, followed by internal attack on the phosphate chain by a coordinated hydroxide ion.

Phosphates play a vital role in the energy-transfer reactions of living systems, and as a result, an understanding of their chemistry, especially hydrolytic reactions, is of fundamental importance. The ability of coordinated metal ions, particularly cobalt(III), to catalyze the hydrolysis of both inorganic and biological phosphates has been demonstrated by several groups of workers.[1-4] A variety of different effects has been suggested[5] to account for these accelerations, and the purpose of the research

(1) Cornelius, R. D., *Inorg. Chem.* **1980**, *19*, 1286.
(2) Hubner, P. W. A.; Milburn, R. M. *Inorg. Chem.* **1980**, *19*, 1267.
(3) Suziki, S.; Higashiy, T.; Nakahara, A. *Bioinorg. Chem.* **1978**, *8*, 277.

0002-7863/82/1504-2356$01.25/0